Diagnosis tools for humidity-born surface contaminants on Li[$Ni_{0.8}Mn_{0.1}Co_{0.1}$]O_2 cathode materials for lithium batteries

Annika R. Schuer [a,b], Matthias Kuenzel [a,b], Shuo Yang [c], Malte Kosfeld [c], Franziska Mueller [c], Stefano Passerini [a,b,**], Dominic Bresser [a,b,*]

[a] Helmholtz Institute Ulm (HIU), Helmholtzstrasse 11, 89081, Ulm, Germany
[b] Karlsruhe Institute of Technology (KIT), P.O. Box 3640, 76021, Karlsruhe, Germany
[c] Volkswagen AG, Berliner Ring 2, 38440, Wolfsburg, Germany

HIGHLIGHTS

- Development of diagnosis tools for Ni-rich Li-ion cathodes.
- Investigation of the impact of humidity exposure during storage.
- Warder titration as suitable method for the determination of carbonates.
- Verification of the suitability of the diagnosis tools by electrochemical tests.

GRAPHICAL ABSTRACT

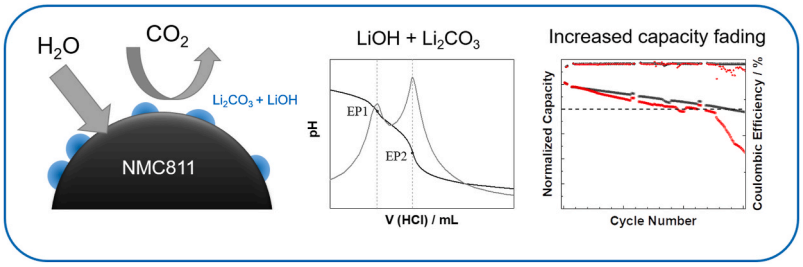

ARTICLE INFO

Keywords:
Ni-rich NMC
Cathode
Titration
Humidity
Lithium battery

ABSTRACT

Ni-rich layered oxides such as Li[$Ni_{0.8}Mn_{0.1}Co_{0.1}$]O_2 (NMC_{811}) are highly sensitive towards moisture. Any contact with humidity leads to the formation of surface contaminants, which reflect into an increased overpotential and cause accelerated capacity loss during cycling. This is particularly relevant when considering large-scale processing. Herein, we report a diagnostic set of tools to rapidly assess the extent of such surface contaminants on Ni-rich NMC materials comprising different titration methods, electron microscopy, and the determination of the reversible and irreversible water adsorption. Based on a series of samples subjected to a controlled humidity for varying times, the formation of carbonate and hydroxide species is investigated and correlated to the eventual electrochemical performance in half-cells and full-cells. The results show that even rather short storage times under humid atmosphere lead to substantial water uptake and surface species formation and that the formation of these surface species has a severe impact on the capacity retention in half-cells and graphite||NMC_{811} full-cells.

1. Introduction

During the past decades, lithium-ion batteries (LIBs) have become one of the most important energy storage technology for our everyday life [1–3]. Besides already powering all kinds of portable electronics, LIBs are enabling the mass market introduction of electric vehicles (EVs)

* Corresponding author. Helmholtz Institute Ulm (HIU), Helmholtzstrasse 11, 89081, Ulm, Germany.
** Corresponding author. Helmholtz Institute Ulm (HIU), Helmholtzstrasse 11, 89081, Ulm, Germany.
E-mail addresses: stefano.passerini@kit.edu (S. Passerini), dominic.bresser@kit.edu (D. Bresser).

[4–6]. To qualify for the application in EVs, however, the utilized active materials have to provide high specific capacities in combination with suitable de-/lithiation potentials to yield high energy densities accompanied by long lifetimes and, ideally, low cost [7]. Presently, the active materials of choice for the positive electrode in today's and near-/-mid-term future LIBs are layered lithium metal oxides such as Li$[Ni_xMn_yCo_z]O_2$ (NMC) and Li$[Ni_xCo_yAl_z]O_2$ (NCA) as well as spinel-type $LiNi_{0.5}Mn_{1.5}O_4$; the latter one being especially interesting with regard to the absence of Co and the relatively low Ni content [8–10]. Of particular industrial interest, at present, is Ni-rich NMC with a Ni content of ≥80% and a theoretical specific capacity of >200 mA h g^{-1} [11–13]. However, these materials suffer of the very high sensitivity towards moisture, leading to severe capacity fading and performance loss of materials that have not been stored and processed under strictly dry conditions, which represents one of the great challenges towards the large-scale production of Ni-rich NMC-based LIBs [14]. Precisely, the high reactivity of these materials toward moist air results in the formation of lithium and transition metal (especially nickel) bearing impurities such as hydroxides and carbonates [15–17], accompanied by Li^+/H^+ exchange [18, 19]. The consequent loss of electrochemically active lithium leads to a drop in reversible capacity [20–22], while the simultaneously formed lithium and nickel hydroxides react further to lithium and nickel carbonate with CO_2 from the ambient atmosphere [23–25]. For lithium, the process is summarized below:

$$Li^+ + H_2O \rightarrow H^+ + LiOH \quad (1)$$

$$LiOH + CO_2 \rightarrow LiHCO_3 \quad (2)$$

$$LiOH + LiHCO_3 \rightarrow H_2O + Li_2CO_3 \quad (3)$$

The formation of such surface impurities consumes lithium and nickel from the active material. Additionally, the presence of the metal carbonates causes moreover electrolyte decomposition during cycling, resulting in the formation of, e.g., harmful and corrosive HF as well as gaseous CO_2 [26–28]. These effects have been well investigated already for the long-term storage (months to years) of Ni-rich NMC, its washing (not least to remove such surface species), and its aqueous processing into electrodes. All these rather harsh treatments or conditions showed considerable consequences on the performance of the material in the battery cell [16,29,30]. What remains to be studied, however, is the effect of relatively short (hours to days) exposure to moist atmosphere, for instance, during packaging, handling, and/or storage. In fact, even small amounts of surface impurities might have a significant effect on the cycling behavior and battery cell lifetime. Additionally, surface impurities such as metal carbonates have a detrimental effect on the processability of the material due to the gelation during slurry preparation [22,31]. Accordingly, it is of fundamental interest for battery manufacturers to develop suitable, easy to implement, and rapid methodologies to evaluate the quality of such materials before processing them into electrodes.

Herein, we report a comprehensive analysis of Ni-rich NMC active materials that have been exposed for defined times to a carefully controlled humidity level. This analysis comprises amongst others the determination of the reversibly absorbed water as well as the quantification of the waterborne surface species such as LiOH and Li_2CO_3 via a facile titration method, allowing a fast evaluation of the quality of the cathode active material powder. This is eventually confirmed by electrochemical tests of such materials in half-cells and full-cells with graphite-based anodes, corroborating the importance of developing suitable quality measures.

2. Experimental

2.1. Ageing of Ni-rich NMC under controlled conditions

The fresh commercial Ni-rich NMC powder was stored as-received in an Ar-filled glove box (MBraun) with a H_2O and O_2 content of <0.1 ppm to prevent any (further) reaction with the atmosphere. For the controlled aging, part of the powder was stored for up to 7 days in a specifically designed humidity chamber, making use of the principle of deliquescence relative humidity (RH). This is achieved by placing an over-saturated salt solution in a closed chamber, so that an equilibrium forms between the crystalline salt, its solution, and the RH in the humidity chamber. The atmosphere in the humidity chamber corresponded with the ambient atmosphere with oxygen and carbon dioxide levels of about 21 vol% and 0.04 vol%, respectively. For the over-saturated solution, $NaNO_2$ was used, which provides a constant RH of 65% at 25 °C [32]. Fig. 1 depicts a schematic illustration of the utilized setup.

2.2. Physicochemical characterization

The water content of the active material powders was determined by indirect Coulometric Karl-Fischer titration (C30, Mettler-Toledo with drying oven DO308). For this purpose, 0.2–0.5 g of powder was heated for 10 min at 170 °C in a tubular drying oven. The released water was transferred to the Karl-Fischer titrant solution via an argon gas stream. Complementarily, thermogravimetric analysis (TGA) was carried out on a sorption analysis device (Q5000SA, TA Instruments) to determine the water content. For this purpose, the humidity in the sample chamber was set to 0% and the sample was dried for 5 h at 60 °C, while the mass loss was recorded. Subsequently, sorption curves were recorded using the same instrument. After the isothermal step at 0% RH, the humidity was increased in steps of 0.2% min^{-1} until 65% RH was reached and then decreased again to 0% RH. Dry nitrogen gas was used as the carrier gas. The error for the Karl-Fischer and TGA experiments was calculated by determining the standard deviation of the mean value of the repeated experiments (at least three measurements per experiment were conducted).

The carbonate and hydroxide content were determined according to the Warder titration using a Metrohm Omnis titrator. The samples were prepared in an argon-filled glove box (Bel-Art). For each set of measurements, 5 g of powder were suspended in 100 mL degassed ultra-pure water (Millipore). After stirring for 2 min at 300 rpm, the dispersion was filtered for 5 min. 10 mL of the filtrate was poured into the titration vessel, which was then transferred to the titrator using an air-tight lid to avoid any contact with the surrounding air. The titration vessel was connected air-tightly to the titrator and flushed with argon during the measurement. For the titration, 0.05 mol L^{-1} HCl was added at a dosing rate of 1 mL min^{-1} under continuous stirring. The equivalence points, indicating the hydroxide and carbonate content, were determined as the maxima of the derivative of the titration curve. Additionally, scanning electron microscopy (SEM) micrographs were obtained by means of a Zeiss Crossbeam 340 field-emission electron microscope.

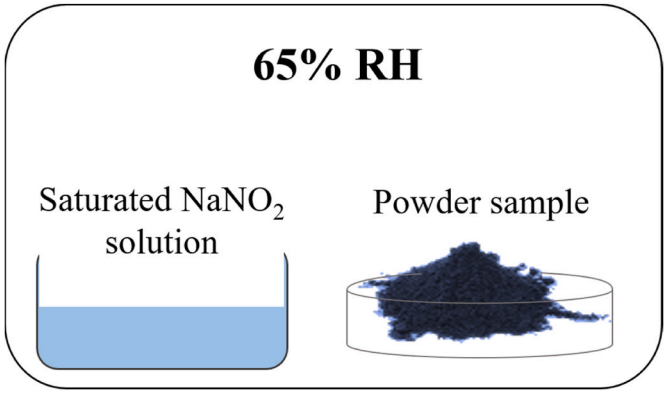

Fig. 1. Schematic representation of the humidity chamber used for ageing the Ni-rich NMC powder at 65% relative humidity (RH) for up to 7 days.

2.3. Electrode preparation

Electrodes were prepared with an active material (Ni-rich NMC) to conductive agent (carbon black and graphite) to binder (polyvinylidene difluoride, PVdF) mass ratio of 94:4:2. *N*-methyl-2-pyrrolidone (NMP; anhydrous, >99.5%, Sigma-Aldrich) was used as a solvent for preparing the binder solution and as dispersant for the slurry preparation (70 wt% solid content) using a planetary centrifugal high-speed mixer (Wellcos, Non-Bubbling Kneader NBK-1). The cathode tapes were cast on battery-grade aluminum foil (15 μm, Showa Denko) by means of a laboratory doctor blade equipment. After pre-drying for 2 h at 80 °C, the electrode sheets were transferred to the dry room with a dew point of less than 70 °C and stored there overnight. For the half-cell tests, circular electrodes (diameter: 12 mm, active material mass loading: 12.9–14.0 mg cm^{-2}) were punched and pressed to reach an electrode density of ~2.8 g cm^{-3}. For the full-cell tests, the Ni-rich NMC positive electrodes (active material mass loading: 12.9–13.1 mg cm^{-2}) with an area of 9 cm^2 were punched and calendared to reach an average electrode density of around ~2.6 g cm^{-3} after drying under vacuum for 12 h at 120 °C prior to the cell assembly.

The negative electrodes comprised 95 wt% of graphite (Actilion, Imerys), 4 wt% of conductive carbon (SuperC45, Imerys), and 1 wt% of binder (one part carboxymethyl cellulose, CMC (WALOCEL™ CRT 2000 PPA 12, Dow Wolff Cellulosics), and three parts styrene butadiene rubber, SBR). The aqueous electrode slurry (50 wt% solid content) was mixed using a magnetic stirrer, followed by 10 min homogenization at 5000 rpm utilizing a DREMEL 4000. After degassing, the aqueous slurry was cast on copper foil (10 μm thickness, Showa Denko) and the coated sheets were pre-dried for 12 h at 80 °C before cutting electrodes with an area of 10.89 cm^2 and an active material mass loading of 8.5–10.2 mg cm^{-2} for the full-cell tests. The negative electrodes were densified to around 1.1 g cm^{-3} after the final drying for 12 h at 120 °C under vacuum.

2.4. Cell assembly and electrochemical characterization

The electrochemical characterization in half-cells was carried out using coin-cells (CRT2030), which were assembled in an argon-filled glove box with a H_2O and O_2 level of <0.1 ppm. The counter electrodes were lithium metal disks with a thickness of 500 μm (battery grade, Honjo). The glass fiber separator (Whatman, GF/D, 670 μm) was soaked with 100 μL of the electrolyte (1 M $LiPF_6$ in EC:DMC, 1:1 by volume, UBE). The positive electrodes were tested with cut-off voltages of 3.0 V and 4.35 V at 1C after an initial formation cycle (CC-CV) from OCV to 4.3 V at 0.1C followed by a CV step (i < C/20, max. 1 h; 1C ≈ 200 mA g^{-1}). Single-layer pouch cells were used for the validation in graphite||Ni-rich NMC full-cells and assembled in the dry room. The olefin separators were soaked with 800 μL of the electrolyte. The N:P ratio was about 1.2 based on the reversible specific capacities in the 5th cycle at C/10, as obtained from the half-cell tests. In the case of graphite, the tests were performed in coin cells with one formation cycle from OCV to 0.02 V at C/10 in CC-CV mode (i < C/20 for max. 3 h; 1C ≈ 370 mA g^{-1}) and subsequent cycling between 0.02 V and 1.5 V at varying dis-/charge rates. Following the formation cycles at 20 °C, the cells were cycled under rather intense conditions, i.e., at 45 °C, with a CC-CV testing protocol (cut-off voltages: 3.0 V and 4.25 V; CC step at 1C; CV step at 4.25 V till i < C/20, max. 3 h). The capacity delivered in the last formation cycle is assumed as the nominal cell capacity for the C rate determination. During the cycling test, 3 cycles at C/3 were intermitted every 50 cycles. For each experiment, at least five cells were studied to ensure the reproducibility of the results.

3. Results and discussion

The Ni-rich NMC powder was stored for up to 7 days under controlled humidity (65% RH) and temperature (25 °C) conditions in an isolated climatic chamber (Fig. 1). The water content of the powders was determined via Karl-Fischer titration immediately after removal from the climatic chamber, prior to storing them in an Ar-filled glove box.

The results are summarized in Table 1. In the case of the pristine material and the 7d aged material, additionally, TGA was performed to crosscheck the results (Fig. 2). In fact, the values from both methods are in good agreement with 71 ± 31 ppm (Karl-Fischer titration) and 53 ± 15 ppm (TGA) for the pristine material as well as 379 ± 36 ppm (Karl-Fischer titration) and 398 ± 2 ppm (TGA) for the 7d-aged material, with the deviation being well within the experimental error. This good match is particularly noteworthy, as the Karl-Fischer titration is performed in the dry room with a water content of about 2.6 ppm by volume, while the sample examined by TGA is very shortly exposed to the ambient atmosphere when loading the sample into the device. This finding might indicate that the Ni-rich NMC is taking up minor amounts of water very rapidly, even under dry room conditions, and/or it simply contained some adsorbed water in the 'as-received' state. Generally, however, a rapid water uptake is evident also from the other two samples aged for 1 day (362 ± 43 ppm) and 3 days (368 ± 94 ppm) in the humidity chamber, revealing that the majority of the water uptake occurs in the first 24 h.

To obtain further insights into the kinetics of the water-uptake, sorption curves were recorded for the pristine and 7d-aged powders (Fig. 3a). The direct comparison of the curves reveals obvious differences for the water adsorption behavior of the two samples. The pristine sample appears to exhibit a Type III adsorption behavior, while the 7d-aged sample resembles rather a Type II behavior with an initially steeper increase, followed by a change in slope (see **Fig. S1** for the "idealized" isotherms according to IUPAC). The Type III behavior of the pristine sample indicates relatively weak interactions between the adsorbent and the sample and the immediate formation of multilayers of the absorbed molecules on the pristine particle surface [33,34]. Differently, the Type II behavior observed for the 7d aged sample indicates an initial physisorption of the adsorbate until the entire sample surface is covered by a monolayer of the same (here: H_2O) [33]. Subsequently, as marked by the change in slope of the sorption curve, the multilayer formation begins. This different adsorption behavior for the two samples is assigned to the formation of humidity-induced surface species upon storage at 65% RH such as hydroxides and carbonates.

The formation of such surface species is also evident from the SEM analysis of the materials (**Fig. 4**), showing that they are formed already on the 1d-aged material. This further highlights the rather fast reaction upon exposure to humidity [35], as evidenced also by the water absorption experiment conducted for one full day at 65% RH (see Fig. S2). This rapid reaction is moreover reflected by the Type II desorption behavior for both the pristine and the 7d-aged materials (Fig. 3a), although less pronounced for the pristine sample. In part, this is related to the experiment being conducted under N_2 atmosphere, i.e., in absence of CO_2, allowing only for the formation of hydroxides rather than carbonates [35]. Generally, the pristine material adsorbs and desorbs less water than the 7d-aged sample, while it appears that the eventual mass change is more pronounced for the pristine sample, but present for both materials. When applying an additional drying step at 60 °C and 0% RH (**Fig. 3b**), though, it is observed that the mass change for the 7d-aged sample is completely reversible, even slightly negative, while a minor gain in mass remains for the pristine material, amounting to 86 ppm in good agreement with the data obtained by TGA and Karl-Fischer

Table 1
Water content determined by Karl-Fischer titration (performed thrice) for the pristine and aged (i.e., stored for 1 day, 3 days, and 7 days at 65% RH) Ni-rich NMC powders.

	Pristine	Aged 1d	Aged 3d	Aged 7d
Water content	71 ± 31 ppm	362 ± 43 ppm	368 ± 94 ppm	379 ± 36 ppm

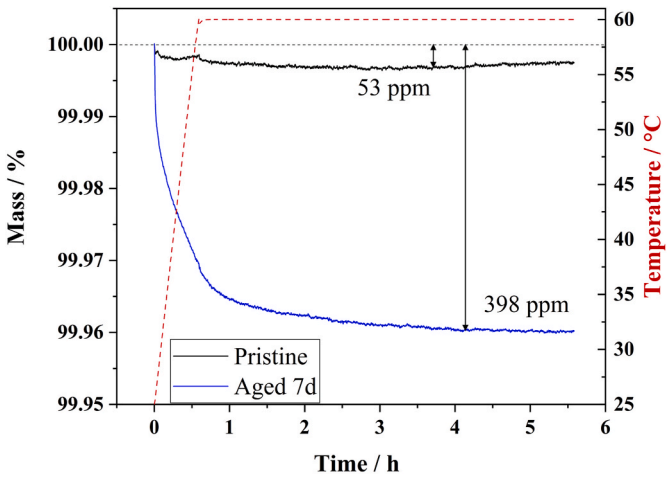

Fig. 2. TGA-derived mass loss of the pristine and 7d aged Ni-rich NMC powder upon drying at 60 °C and 0% RH.

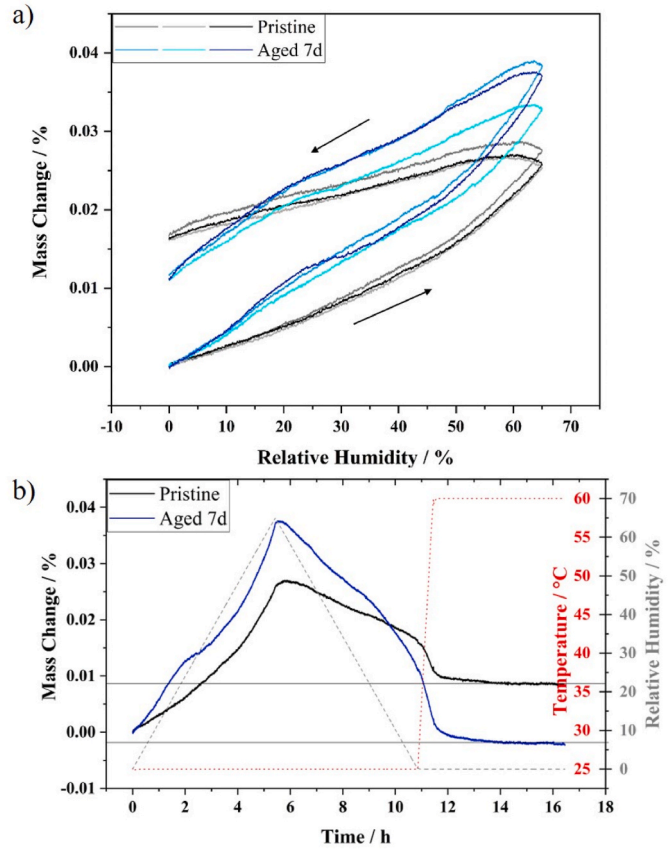

Fig. 3. (a) Sorption curves for the same powders recorded for a steady increase of the RH from 0% RH to 65% RH and back (as indicated by the arrows). Three measurements were collected for each sample. (b) Sorption curves of the pristine and 7d aged Ni-rich NMC as a function of time with a subsequent drying step at 60 °C and 0% RH.

titration. These differences are assigned to the initial presence of surface-covering hydroxides and carbonates in the case of the 7d aged sample and their (fully reversible) reaction with additional water in the absence of CO_2; thus, not allowing for the transformation of hydroxides into carbonates. In the case of the pristine sample, however, the formation of LiOH is (partially) irreversible and it remains on the particle surface, while the physically adsorbed water is released again upon drying.

Overall, the comparative investigation via Karl-Fischer titration and gravimetric analyses nicely illustrates the high water-sensitivity of Ni-rich NMC and provides a quantification of the reversibly and irreversibly adsorbed water and surface species formed. Nevertheless, the gravimetric methods do not allow for a selective quantitative determination of the hydroxides and carbonates formed upon storage in a humid environment. For this purpose, the Warder titration method was adapted, allowing for the simultaneous quantification of hydroxides and carbonates by acid-base titration with aqueous HCl [36]. It is noted here that this method is anion-specific, i.e., it does not differentiate between different cations such as lithium or nickel. Nevertheless, it is a very simple and yet powerful technique. To start with, the Ni-rich NMC was stirred in deaerated water to dissolve the carbonates and hydroxides and the resulting filtrate was titrated. By measuring the volume of HCl at the equivalence points (EPs) of the titration curve, which are determined via the 1st derivative (see Fig. S2), the concentration of hydroxides and carbonates was calculated using the following equations [37]:

$$c\ (OH^-)\quad (2V_1\quad V_2)*c\ (HCl)*\frac{1}{V_{sample}} \tag{4}$$

$$c\ (CO_3^{2-})\quad (V_2\quad V_1)*c\ (HCl)*\frac{1}{V_{sample}} \tag{5}$$

An important parameter is the initial stirring time to dissolve the surface hydroxides and carbonates. To investigate its impact, we varied the stirring time from 2 to 5–10 min. The results, presented in Table S1, reveal that the carbonate content remains essentially constant, while the hydroxide content is increasing with an increasing stirring time. In fact, the careful sample preparation and titration in an CO2-free atmosphere prevents any additional carbonate formation, while the formation of hydroxides such as LiOH cannot be prevented. This finding is in good agreement with previous studies, which reported that the Li^+/H^+ exchange occurs even during a short contact with water, leading to the formation of LiOH [29,38]. Pritzl et al. [39], for instance, investigated the effect of washing Ni-rich NMC to remove the surficial hydroxides and carbonates owing to their detrimental impact on the cycling stability. In the first washing step, they found 6400 ppm of Li_2CO_3 and 4600 ppm LiOH. In the second washing step, they still detected 2800 ppm of LiOH. Assuming that all surface impurities were removed upon the first washing step, the LiOH detected after the second washing step had been formed during stirring in water. Therefore, the stirring time was kept as short as possible, i.e., 2 min, which appeared to be sufficient to dissolve all carbonate species, while keeping in mind that the hydroxide content is presumably slightly overestimated.

Representative titration curves for the pristine and 7d-aged samples are shown in Fig. 5 and the corresponding hydroxide and carbonate contents are summarized in Table 2. The carbonate content increased from 577 ppm for the pristine sample to 919 ppm for the 7d-aged sample, illustrating the continuous reaction with the humid atmosphere upon storage. The hydroxide content, however, slightly decreased from 2722 ppm for the pristine sample to 2611 ppm for the 7d-aged sample. This finding is in line with the reactions summarized in equations (1)–(3), since the initially present hydroxides are converted into carbonates in presence of CO_2. In fact, if we assume, for instance, that all the hydroxides formed during the sorption measurement (86 ppm; Fig. 2) are converted into carbonates, this value is in good agreement with the difference in carbonate species detected for the pristine and the 1d aged sample, i.e., 91 ppm, according to the Warder titration method. Summarizing, these findings show that even a very short exposure of Ni-rich NMC to humidity and CO_2 results in the rapid formation of hydroxide and carbonate species at the powder surface.

Finally, we also studied the impact of the 7 days storage of Ni-rich NMC powder under controlled humidity on the electrochemical performance of Ni-rich NMC electrodes and compared it with that of electrodes made with the pristine Ni-rich NMC powder. The normalized half-

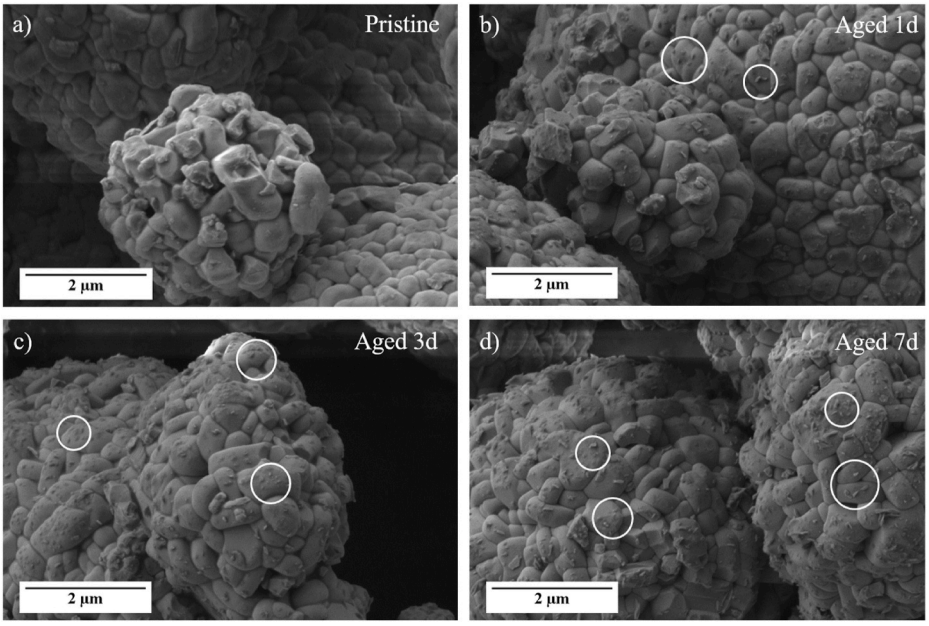

Fig. 4. SEM micrographs of (a) the pristine Ni-rich NMC and (b–d) the samples aged for (b) 1 day, (c) 3 days, and (d) 7 days. The white circles highlight the surface species that are formed upon exposure to humidity.

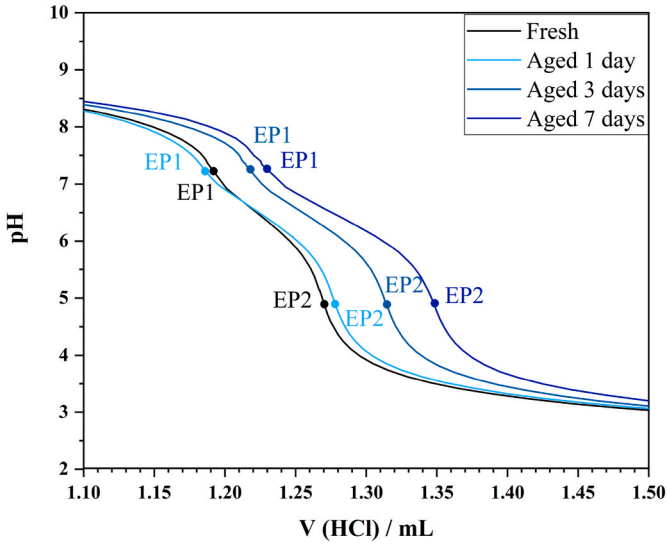

Fig. 5. Titration curves recorded for the pristine Ni-rich NMC as well as the samples aged for 1 day, 3 days, and 7 days at 65% RH with an indication of the equivalence points (EPs) located at pH values of about 7.3 and 4.8, as determined from the first derivative of the pH curves (see Fig. S3).

Table 2
Carbonate and hydroxide content determined by the Warder titration for the pristine Ni-rich NMC as well as the samples aged for 1 day, 3 days, and 7 days.

	Pristine	1d Aged	3d Aged	7d Aged
OH	2722 ± 47 ppm	2654 ± 35 ppm	2629 ± 61 ppm	2611 ± 37 ppm
CO_3^{2}	577 ± 46 ppm	668 ± 31 ppm	691 ± 42 ppm	919 ± 44 ppm

cell test results are presented in Fig. 6. The dis/charge profiles of the first cycle at C/10 (Fig. 6a) are essentially superimposed apart from the initial activation barrier observed for 7d-aged Ni-rich NMC at about 3.75 V upon charge and a slightly lower capacity in the case of the 7d-aged sample owing to the formation of LiOH and Li2CO3 (the latter is not shown herein owing to the normalization for the sake of comparability). This is associated with the presence of surface impurities such as Li_2CO_3 [16]. Upon subsequent cycling at 1C (**Fig. 6b**) the capacity fading is more pronounced for the 7d-aged Ni-rich NMC electrode with a significant decay after 30 cycles. After 50 cycles, the cell comprising the 7d-aged active material exhibited capacity retention of only 87% compared to 90% for the pristine Ni-rich NMC electrode. This higher capacity fade originates from a higher cell polarization, as indicated by the comparison of the 50th cycle voltage profiles in Fig. 6c, which may be assigned to the reaction of the surface impurities with the electrolyte leading to a larger amount of gas formation and, most important, the formation of HF attacking the active material, leading to the buildup of a more resistive interphase [15,40].

The following electrochemical tests were performed on Li-ion cells at an elevated temperature of 45 °C, i.e., rather harsh conditions, to better highlight the differences between the electrodes made with the pristine and 7d-aged materials (Fig. 7). The cell comprising the 7d-aged Ni-rich NMC as active material shows an inferior capacity throughout the whole cycle test (150 cycles). Additionally, it shows a pronounced capacity fading hitting the 80% capacity retention limit after 110 cycles. The fading increases even more rapidly after about 120 cycles leading to a dramatic capacity drop. Differently, the Li-ion cell comprising the pristine Ni-rich NMC reveals a rather stable cycling and hits the 80% capacity retention significantly later, i.e., after ca. 140 cycles. The inset in Fig. 7, depicting a comparison of the corresponding dis-/charge profiles for a few selected cycles, illustrates that the fading of the electrode made with the 7d-aged Ni-rich NMC originates once more from a greater cell polarization.

4. Conclusions

The herein reported combination of gravimetric and titration methods accompanied by electron microscopy provides a suitable set of diagnostic tools for the quality assessment of Ni-rich NMC cathode active materials in order to determine the potential exposure to humid atmosphere during the material processing, handling, and storage, even for rather short time. The controlled aging at 65% RH for 1 day, 3 days, and 7 days reveals a continuous increase in surface impurities and the rapid conversion of hydroxides into carbonates, which can be

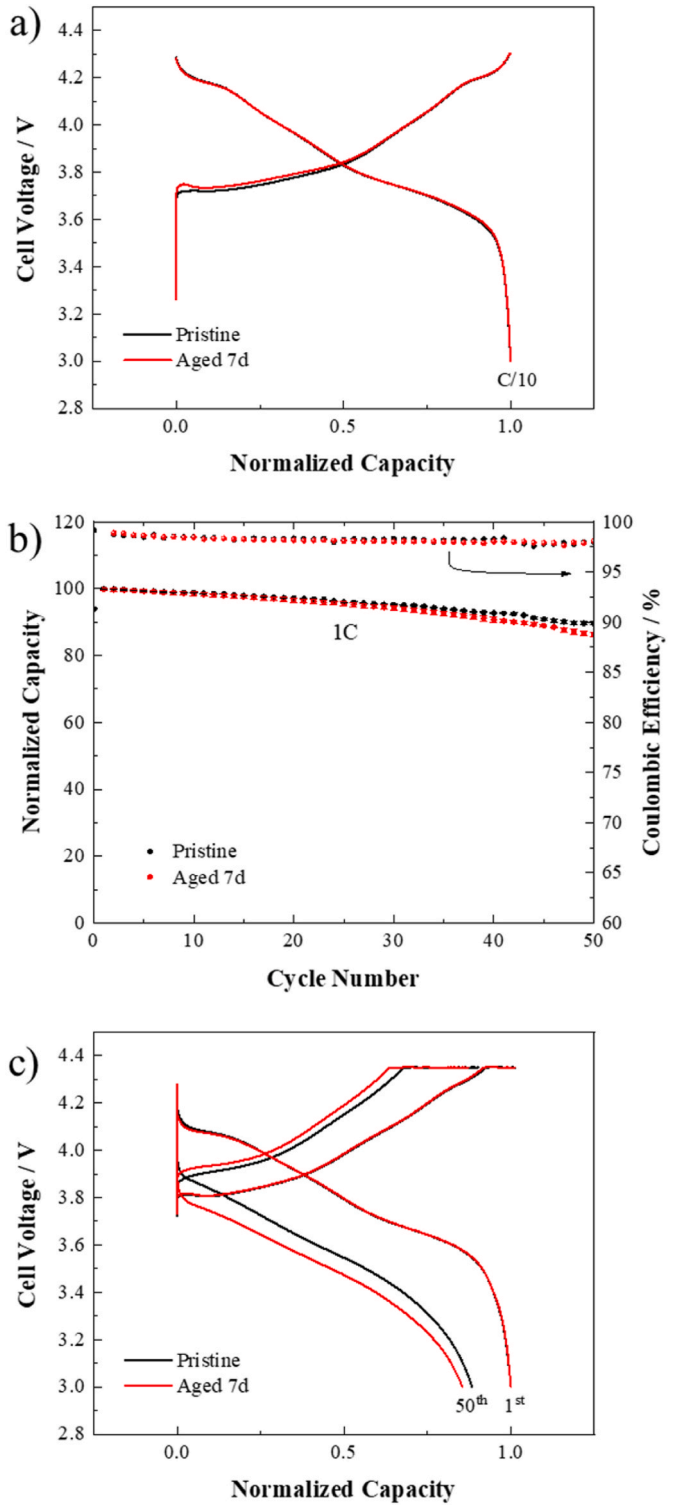

Fig. 6. (a) Dis-/charge profiles for the initial formation cycle at C/10 (incl. a CV step at the end of the charge process with i < C/20, max. 1 h) of half-cells with pristine (in black) and 7d aged (in red) Ni-rich NMC as the active material for the positive electrode (T = 20 °C); the capacity was normalized based on the first reversibly obtained discharge capacity. (b) Plot of the normalized capacity and Coulombic efficiency as a function of the cycle number at a constant dis-/charge rate of 1C after the formation cycle at C/10. (c) Comparison of the dis-/charge profiles for the 1st and 50th cycle for the two different half-cells at 1C. (For interpretation of the references to colour in this figure legend, the reader is referred to the Web version of this article.)

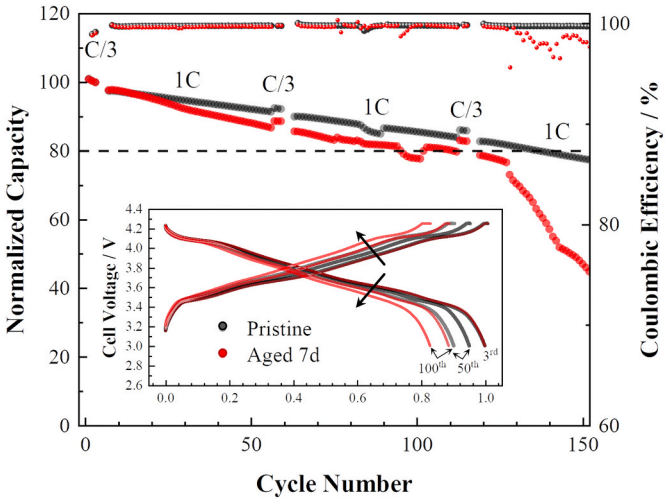

Fig. 7. Plot of the normalized capacity as a function of the cycle number for graphite||NMC_{811} full-cells cycled at 45 °C after three formation cycles at T = 20 °C, comprising the pristine Ni-rich NMC (in black) and 7d aged Ni-rich NMC (in red) as the active material for the positive electrode (the horizontal dashed line indicates a capacity retention of 80%); as inset are provided selected voltage profiles, i.e., the 3rd, 50th, and 100th cycle. (For interpretation of the references to colour in this figure legend, the reader is referred to the Web version of this article.)

quantitatively determined by the Warder titration method. The presence of these surface impurities results in the inferior electrochemical performance – particularly in lithium-ion cells. We may anticipate that these findings will add to the development of a rapid and easy quality control of water-sensitive active materials prior to the electrode preparation and cell assembly, which is critical for cell manufacturers.

CRediT authorship contribution statement

Annika R. Schuer: Methodology, Investigation, Validation, Formal analysis, Visualization, Writing – original draft. **Matthias Kuenzel:** Methodology, Investigation, Validation, Formal analysis, Visualization, Writing – original draft, Writing – review & editing. **Shuo Yang:** Conceptualization, Methodology, Formal analysis, Resources, Writing – review & editing. **Malte Kosfeld:** Methodology, Formal analysis, Resources, Writing – review & editing. **Franziska Mueller:** Conceptualization, Methodology, Formal analysis, Resources, Writing – review & editing. **Stefano Passerini:** Conceptualization, Methodology, Resources, Writing – review & editing, Supervision, Funding acquisition. **Dominic Bresser:** Conceptualization, Methodology, Resources, Writing – original draft, Writing – review & editing, Supervision, Project administration, Funding acquisition.

Declaration of competing interest

The authors declare that they have no conflict of interest.

Acknowledgement

A.R.S., M. Ku., S.P., and D.B. would like to acknowledge financial support from Volkswagen AG, the Helmholtz Association, and the German Federal Ministry of Education and Research (BMBF) within the ExcellBattUlm project (03XP0257D).

References

[1] M. Armand, J.M. Tarascon, Nature 451 (2008) 652–657.
[2] M. Marinaro, D. Bresser, E. Beyer, P. Faguy, K. Hosoi, H. Li, J. Sakovica, K. Amine, M. Wohlfahrt-Mehrens, S. Passerini, J. Power Sources 459 (2020) 228073.
[3] D. Bresser, K. Hosoi, D. Howell, H. Li, H. Zeisel, K. Amine, S. Passerini, J. Power Sources 382 (2018) 176–178.
[4] P.A. Eisenstein, NBCnews, "GM is going all electric, will ditch gas- and diesel-powered cars," can be found under. https://www.nbcnews.com/business/autos/gm-going-all-electric-will-ditch-gas-diesel-powered-cars-n806806, 2017.
[5] I. Europe, Volkswagen to go all electric by 2026," can be found under. https://industryeurope.com/volkswagen-to-go-all-electric-by-2026/, 2019.
[6] Volvo, Volvo Cars to go all electric," can be found under. https://www.media.volvocars.com/global/en-gb/media/pressreleases/210058/volvo-cars-to-go-all-electric, 2017.
[7] M. Armand, P. Axmann, D. Bresser, M. Copley, K. Edstrom, C. Ekberg, D. Guyomard, B. Lestriez, P. Novák, M. Petranikova, W. Porcher, S. Trabesinger, M. Wohlfahrt-Mehrens, H. Zhang, J. Power Sources 479 (2020) 228708.
[8] H.J. Noh, S. Youn, C.S. Yoon, Y.K. Sun, J. Power Sources 233 (2013) 121–130.
[9] M. Kuenzel, G.-T.T. Kim, M. Zarrabeitia, S.D. Lin, A.R. Schuer, D. Geiger, U. Kaiser, D. Bresser, S. Passerini, Mater. Today 39 (2020) 127–136.
[10] M. Wentker, M. Greenwood, J. L, Energies 12 (2019) 1–18.
[11] A. Manthiram, J.C. Knight, S.T. Myung, S.M. Oh, Y.K. Sun, Adv. Energy Mater. 6 (2016).
[12] J. Zheng, W.H. Kan, A. Manthiram, ACS Appl. Mater. Interfaces 7 (2015) 6926–6934.
[13] M. Greenwood, M. Wentker, J. Leker, J. Power Sources Adv. 9 (2021) 100055.
[14] P. Rozier, J.M. Tarascon, J. Electrochem. Soc. 162 (2015) A2490–A2499.
[15] J. Sicklinger, M. Metzger, H. Beyer, D. Pritzl, H.A. Gasteiger, J. Electrochem. Soc. 166 (2019) A2322–A2335.
[16] R. Jung, R. Morasch, P. Karayaylali, K. Phillips, F. Maglia, C. Stinner, Y. Shao-Horn, H.A. Gasteiger, J. Electrochem. Soc. 165 (2018) A132–A141.
[17] A.C. Martinez, S. Grugeon, D. Cailleu, M. Courty, P. Tran-Van, B. Delobel, S. Laruelle, J. Power Sources 468 (2020) 1–10.
[18] I.A. Shkrob, J.A. Gilbert, P.J. Phillips, R. Klie, R.T. Haasch, J. Bareno, D. P. Abraham, J. Electrochem. Soc. 164 (2017) A1489–A1498.
[19] I. Hamam, N. Zhang, A. Liu, M.B. Johnson, J.R. Dahn, J. Electrochem. Soc. 167 (2020) 130521.
[20] I. Doberdò, N. Loffler, N. Laszczynski, D. Cericola, N. Penazzi, S. Bodoardo, G. T. Kim, S. Passerini, J. Power Sources 248 (2014) 1000–1006.
[21] D.-H. Cho, C.-H. Jo, W. Cho, Y.-J. Kim, H. Yashiro, Y.-K. Sun, S.-T. Myung, J. Electrochem. Soc. 161 (2014) A920–A926.
[22] D. Bresser, D. Buchholz, A. Moretti, A. Varzi, S. Passerini, Energy Environ. Sci. 11 (2018) 3096–3127.
[23] M. Wood, J. Li, R.E. Ruther, Z. Du, E.C. Self, H.M. Meyer, C. Daniel, I. Belharouak, D.L. Wood, Energy Storage Mater. 24 (2020) 188–197.
[24] H. Liu, Y. Yang, J. Zhang, J. Power Sources 162 (2006) 644–650.
[25] K. Matsumoto, R. Kuzuo, K. Takeya, A. Yamanaka, J. Power Sources 81–82 (1999) 558–561.
[26] M. Bichon, D. Sotta, N. Dupré, E. De Vito, A. Boulineau, W. Porcher, B. Lestriez, ACS Appl. Mater. Interfaces 11 (2019) 18331–18341.
[27] S.E. Renfrew, B.D. McCloskey, J. Am. Chem. Soc. 139 (2017) 17853–17860.
[28] M. Kuenzel, D. Bresser, T. Diemant, D.V. Carvalho, G.T. Kim, R.J. Behm, S. Passerini, ChemSusChem 11 (2018) 562–573.
[29] I. Hamam, N. Zhang, A. Liu, M.B. Johnson, J.R. Dahn, J. Electrochem. Soc. 167 (2020) 130521.
[30] M. Hofmann, M. Kapuschinski, U. Guntow, G.A. Giffin, J. Electrochem. Soc. 167 (2020) 140512.
[31] F. Tsai, J. Jhang, H. Hsieh, C. Li, J. Power Sources 310 (2016) 47–53.
[32] T.P. Labuza, A. Kaanane, J.Y. Chen, J. Food Sci. 50 (1985) 385–392.
[33] M. Thommes, K. Kaneko, A.V. Neimark, J.P. Olivier, F. Rodriguez-Reinoso, J. Rouquerol, K.S.W. Sing, Pure Appl. Chem. 87 (2015) 1051–1069.
[34] C.H. Giles, A.P. D'Silva, I.A. Easton, J. Colloid Interface Sci. 47 (1974) 766–778.
[35] L. Zou, Y. He, Z. Liu, H. Jia, J. Zhu, J. Zheng, G. Wang, X. Li, J. Xiao, J. Liu, J. G. Zhang, G. Chen, C. Wang, Nat. Commun. 11 (2020) 3204, https://doi.org/10.1038/s41467-020-17050-6.
[36] C. Winkler, Praktische Übungen in Der Maßanalyse, Verlag Von A.Felix, Leipzig, 1920.
[37] A.A. Benedetti-Pichler, M. Cefola, B. Waldman, Ind. Eng. Chem. - Anal. Ed. 11 (1939) 327–332.
[38] J. Paulsen, J. Kim, US Patent, 2014. US 20140054495A1.
[39] D. Pritzl, T. Teufl, A.T.S. Freiberg, B. Strehle, J. Sicklinger, H. Sommer, P. Hartmann, H.A. Gasteiger, J. Electrochem. Soc. 166 (2019) A4056–A4066.
[40] N. V Faenza, L. Bruce, Z.W. Lebens-Higgins, I. Plitz, N. Pereira, L.F.J. Piper, G. G. Amatucci, J. Electrochem. Soc. 164 (2017) A3727–A3741.